PERGAMON

International Journal of Solids and Structures 38 (2001) 7857–7874

INTERNATIONAL JOURNAL OF SOLIDS and STRUCTURES

www.elsevier.com/locate/ijsolstr

Self-adaptive vibration control of smart composite beams using recurrent neural architecture

Manish T. Valoor [a], K. Chandrashekhara [a,*], Sanjeev Agarwal [b]

[a] *Department of Mechanical and Aerospace Engineering and Engineering Mechanics, University of Missouri-Rolla, Rolla, MO 65409, USA*

[b] *Department of Electrical and Computer Engineering, University of Missouri-Rolla, Rolla, MO 65409, USA*

Received 14 September 2000; in revised form 14 May 2001

Abstract

A self-adapting vibration control system is developed for damping augmentation in smart composite beams. The conventional vibration control approaches are limited by the requirement of an explicit and often accurate identification of the system dynamics and subsequent offline design of an optimal controller. In the present study a self-adapting vibration control system is developed. A hybrid system comprised of a dynamic diagonal recurrent neural network (DRNN) and an adaptable feed forward neural network is used to control the beam vibrations. Sensing and actuation are achieved using piezoelectric sensors and actuators. A finite element model based on a higher-order shear deformation theory is used to simulate the vibration response of laminated composite beams with integrated piezoelectric sensors and actuators. The dynamic effects of mass and stiffness of the piezoelectric patches are considered in the model. The performance of the DRNN controller is verified for arbitrary initial conditions and loadings. A robustness study including the effects of tip mass, structural parameter variation and partial loss of sensor output is performed. The performance with partial failure of control actuation is also examined. It is seen that the robustness and control capabilities of the hybrid control system are excellent.

Keywords: Composite beam; Piezoelectric sensors and actuators; Vibration control; Finite element; Recurrent neural network

1. Introduction

In recent years, smart composite structures have found their way into a wide variety of applications ranging from ground transportation systems and civil infrastructure to more high technology areas such as spacecrafts. Smart composite structures featuring integrated sensors and actuators with real-time control capabilities provide the structural requirements of high strength, lightweight, high structural damping and low acoustical noise.

Smart structures which have been introduced as an alternative to conventional actively-controlled structures have several distinct advantages. The distributed nature of sensing in smart structures enables

* Corresponding author. Tel.: +1-573-341-4587; fax: +1-573-341-4115.
E-mail address: chandra@umr.edu (K. Chandrashekhara).

0020-7683/01/$ - see front matter
PII: S0020-7683(01)00125-1

accurate sensing of structural response and distributed actuation reduces control spillover problems associated with point actuators. Electrorheological fluids, optical fibers, polyvinylidene film (PVDF), shape memory alloys and piezoceramics have been used as sensors and/or actuators in smart systems. Piezoceramic patches are ideally suited for use as sensors and actuators in vibration control because of low cost and easy implementation. They can be bonded to the surface or embedded within the structure. Crawley and de Luis (1987) and Lee (1990) developed analytical models for surface bonded and embedded piezoelectric actuators. The control system design for such distributed multi-sensor multi-actuator system is, however, more difficult. The conventional vibration control system design requires an explicit and often accurate identification of these multi-input multi-output (MIMO) systems.

The use of neural networks for vibration control has been investigated by several researchers. Flanders et al. (1994) used a radial-basis-function network to minimize beam vibration. Boussalis and Wang (1993) designed a neural network controller based on output feedback to control an antenna-like flexible structure. Chen (1994) implemented neural networks as state estimators in using the modified independent modal space control (MIMSC) algorithm for vibration control of a cantilever beam. Smyser and Chandrashekhara (1997) used neural networks to emulate an LQG/LTR controller for vibration control of composite beams.

Robustness of the control algorithm is one of the primary requirements for structural vibration control. This is because of large variation in structure parameter over the life of its operation and also because of the fact that identification of system dynamics may not be accurate. In this paper neural network architecture is designed and trained to achieve the required control action. An excellent account of neural network for control application can be found in the journal paper by Narendra and Parathasarthi. In the proposed self-adaptive neuro-control architecture, a feed forward identifier network provides the sensitivity information required by the dynamic recurrent neural network (DRNN) controller. The identifier neural network is initially trained offline using data generated by the finite element model, which simulates the vibration response of the beam. In a practical application of the proposed system, the identifier may be trained online by connecting it in parallel with the structure. The DRNN controller is trained using a MIMO modification of the neural network proposed by Ku and Lee (1995). The DRNN controller is trained online and utilizes the sensitivity information of the structure provided by the identifier for weight updates. Once the identifier is trained satisfactorily, the updating of the neural identifier continues during the operation of the system. This accounts for any quasi-static changes in the system dynamics due to structural parameter variations, structural deterioration, loadings, etc. Vibration damping for composite beam using LQG/LTR based robust control and LQG/LTR bared neuro-control has been presented earlier by Varadarajan et al. (2000) and Smyser and Chandrashekhara (1997), respectively. However, both the conventional control and the neuro-control presented lack the ability to adapt with changing beam dynamics. The recurrent neural network band scheme presented in this study tries to address this case of varying beam dynamics.

Neural network hardware in the form of programmable chips allows for easy implementation of the neural networks in a control application (Damle and Rao, 1997). The network memory or weights must simply be programmed into the neural network chips. The neural network controller developed in the present work uses the sensor voltages from the piezoelectric sensors and the previous output of the controller as inputs. The neural controller provides the actuator voltages necessary to minimize the beam vibration. These actuator voltages and the previous sensor voltages constitute the input to the neural identifier.

The performance of the hybrid control system is examined for different initial conditions and loadings. Most practical structures are subjected to various aerodynamic and thermodynamic changes which result in bounded parameter variations in the dynamics of the system. Moreover, the modeling of the system is seldom perfect. The robustness of the proposed system is examined for various structural parameter variations. The massively parallel nature of the neural network hybrid controller enables it to overcome partial failure of the system. In other words, failure or malfunction of a component need not result in a

total failure of the control system. This is illustrated with test cases involving partial loss of sensing or actuation.

2. Mathematical formulation

The laminated composite beam with integrated piezoelectric sensors and actuators considered in the present work is shown in Fig. 1. The beam is of length L, width b and thickness h. The sensors and actuators can be embedded or surface bonded at different locations along the length of the beam. It is assumed that they span the entire width of the beam. Each actuator can be actuated independently, and similarly each sensor output is an independent voltage. Each sensor voltage depends only on the location, the strains, and the piezoelectric material properties.

The beam coordinate axes are shown in Fig. 1. The spatial coordinate x is coincident with the beam axis, the x–y plane coincides with the mid-plane of the beam and the z-axis is defined normal to the midplane according to the right-hand rule. The beam is composed of n laminae oriented at an angle θ_k $(k = 1, \ldots, n)$ with respect to the beam coordinate axes. A higher-order shear deformation theory is used to incorporate the pronounced shear deformation effects which arise due to the high ratio of extension modulus to transverse shear modulus common in laminated composite beams.

2.1. Kinematic relations

The displacement field based on a higher-order shear deformation theory is given by (Smyser and Chandrashekhara (1997))

$$u_1(x,z,t) = u(x,t) + z\left[\phi_x(x,t) - \frac{4}{3}\left(\frac{z}{h}\right)^2\left(\phi_x(x,t) + \frac{\partial w(x,t)}{\partial x}\right)\right]$$
$$u_3(x,z,t) = w(x,t) \tag{1}$$

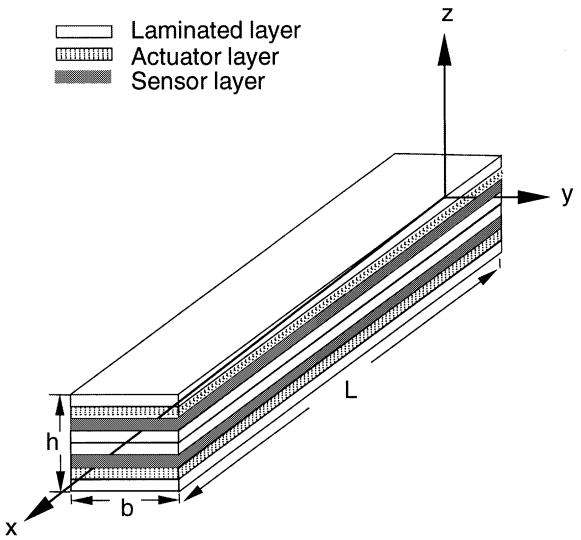

Fig. 1. Laminated beam with integrated piezoelectric sensors and actuators.

where u_1, u_3 denote, respectively, the axial and transverse displacement of a point (x,z) on the beam and $u(x,t)$, $w(x,t)$ denote the axial and transverse displacements of a point $(x,0)$ on the mid-plane of the beam, and $\phi_x(x,t)$ is the normal rotation of a point $(x,0)$ at any instant t.

The strains associated with the above displacement field are

$$\begin{aligned}\varepsilon_x &= \varepsilon_x^0 + z\kappa_x^1 + z^3\kappa_x^2 \\ \gamma_{xz} &= \gamma_{xz}^0 + z^2\kappa_{xz}^2\end{aligned} \tag{2}$$

where

$$\begin{aligned}\varepsilon_x^0 &= \frac{\partial u}{\partial x} \\ \kappa_x^1 &= \frac{\partial \phi_x}{\partial x}; \quad \kappa_x^2 = \frac{-4}{3h^2}\left(\frac{\partial \phi_x}{\partial x} + \frac{\partial^2 w}{\partial x^2}\right) \\ \gamma_{xz}^0 &= \phi_x + \frac{\partial w}{\partial x}; \quad \kappa_{xz}^2 = \frac{-4}{h^2}\left(\phi_x + \frac{\partial w}{\partial x}\right)\end{aligned} \tag{3}$$

The transverse strain and transverse normal stress vanish at the top ($z = h/2$) and bottom ($z = -h/2$) surfaces of the beam. This obviates the need for a shear correction factor, which is normally used in the first-order shear deformation theory.

2.2. Lamina constitutive equations

The equations of motion for a laminated beam accounting for lateral strains is derived by a systematic reduction of two-dimensional constitutive equations.

The lamina constitutive equations incorporating the piezoelectric effect for the kth layer with respect to the laminate (x, y, z) reference axes can be written as (Chandrashekhara and Agarwal, 1993)

$$\{\sigma\}_k = [Q]_k\{\varepsilon\}_k - [e]_k^{\mathrm{T}}\{E\}_k \tag{4}$$

$$\{D\}_k = [e]_k\{\varepsilon\}_k + [\hat{\varepsilon}]_k\{E\}_k \tag{5}$$

where $\{\sigma\}$ is the stress, $[Q]$ is the elastic stiffness matrix, $\{\varepsilon\}$ is the strain and are defined as

$$\{\sigma\} = \{\sigma_x\sigma_y\tau_{yz}\tau_{xz}\tau_{xy}\}^{\mathrm{T}}; \quad \{\varepsilon\} = \{\varepsilon_x\varepsilon_y\gamma_{yz}\gamma_{xz}\gamma_{xy}\}^{\mathrm{T}}; \quad [Q] = \begin{bmatrix} Q_{11} & Q_{12} & 0 & 0 & Q_{16} \\ Q_{12} & Q_{22} & 0 & 0 & Q_{26} \\ 0 & 0 & Q_{44} & Q_{45} & 0 \\ 0 & 0 & Q_{45} & Q_{55} & 0 \\ Q_{16} & Q_{26} & 0 & 0 & Q_{66} \end{bmatrix}$$

$\{E\}$ is the electric field intensity, $\{D\}$ is the electric displacement vector and $[\hat{\varepsilon}]$ is the permittivity matrix. The piezoelectric stress coefficient matrix $[e]$ is expressed in terms of the strain coefficient matrix $[d]$, by the following equation:

$$[e] = [d][Q] \tag{6}$$

Piezoelectric materials possess anisotropic properties. Piezoceramics are polarized in the thickness direction and exhibit transversely isotropic properties in the x–y plane.

For a one-dimensional laminated composite beam, the width (y-direction) is free of stresses (Bhimaraddi and Chandrashekhara, 1991). Therefore $\sigma_y = \tau_{yz} = \tau_{xy} = 0$ while $\varepsilon_y \neq \gamma_{yz} \neq \gamma_{xy} \neq 0$. Using the above constraints in Eq. (5), the constitutive equations can be written as

$$\{\sigma\} = [\overline{Q}]_k\left(\{\overline{\varepsilon}\}_k - \{\overline{d}\}_k E_3^k\right) \tag{7}$$

In the unabridged notation, Eq. (7) can be expressed as

$$\left\{\begin{array}{c}\sigma_x\\ \tau_{xz}\end{array}\right\}_k = \left[\begin{array}{cc}\overline{Q}_{11} & 0\\ 0 & \overline{Q}_{55}\end{array}\right]_k\left(\left\{\begin{array}{c}\varepsilon_x\\ \gamma_{xz}\end{array}\right\}_k - \left\{\begin{array}{c}d_{31}\\ 0\end{array}\right\}_k E_3^k\right) \tag{8}$$

where $\overline{Q}_{11}$ and $\overline{Q}_{55}$ are given by

$$\begin{aligned}\overline{Q}_{11} &= Q_{11} + \left(\frac{Q_{16}Q_{26} - Q_{12}Q_{66}}{Q_{22}Q_{66} - Q_{26}^2}\right)Q_{12} + \left(\frac{Q_{12}Q_{26} - Q_{22}Q_{16}}{Q_{22}Q_{66} - Q_{26}^2}\right)Q_{16}\\ \overline{Q}_{55} &= Q_{55} - \frac{Q_{45}^2}{Q_{44}}\end{aligned} \tag{9}$$

Using the strain displacement relations given by Eq. (2) in Eq. (8) and integrating through the thickness of the beam, the laminate constitutive equation for the beam can be written as

$$\left\{\begin{array}{c}N_x\\ M_x\\ P_x\\ Q_{xz}\\ R_{xz}\end{array}\right\} = \left[\begin{array}{ccccc}\overline{A}_{11} & \overline{B}_{11} & \overline{E}_{11} & 0 & 0\\ \overline{B}_{11} & \overline{D}_{11} & \overline{F}_{11} & 0 & 0\\ \overline{E}_{11} & \overline{F}_{11} & \overline{H}_{11} & 0 & 0\\ 0 & 0 & 0 & \overline{A}_{55} & \overline{D}_{55}\\ 0 & 0 & 0 & \overline{D}_{55} & \overline{F}_{55}\end{array}\right]\left\{\begin{array}{c}\varepsilon_x^0\\ \kappa_x^1\\ \kappa_x^2\\ \gamma_{xz}^0\\ \kappa_{xz}^2\end{array}\right\} - \left\{\begin{array}{c}N_x^p\\ M_x^p\\ P_x^p\\ 0\\ 0\end{array}\right\} \tag{10}$$

where

$$\begin{aligned}\{N_x, M_x, P_x\} &= \int_{-h/2}^{h/2}\sigma_x(1, z, z^3)\,\mathrm{d}z\\ \{Q_{xz}, R_{xz}\} &= \int_{-h/2}^{h/2}\tau_{xz}(1, z^2)\,\mathrm{d}z\\ \{\overline{A}_{11}, \overline{B}_{11}, \overline{D}_{11}, \overline{E}_{11}, \overline{F}_{11}, \overline{H}_{11}\} &= \sum_{k=1}^{n}\int_{z_{k-1}}^{z_k}\overline{Q}_{11}(1, z, z^2, z^3, z^4, z^6)\,\mathrm{d}z\\ \{\overline{A}_{55}, \overline{D}_{55}, \overline{F}_{55}\} &= \sum_{k=1}^{n}\int_{z_{k-1}}^{z_k}\overline{Q}_{55}(1, z^2, z^4)\,\mathrm{d}z\\ \{N_x^p, M_x^p, P_x^p\} &= \sum_{k=1}^{n}\int_{z_{k-1}}^{z_k}\overline{Q}_{11}E_3^k d_{31}(1, z, z^3)\,\mathrm{d}z\end{aligned} \tag{11}$$

and n is the number of layers.

The electric field strength E_3^k is given by

$$E_3^k = \frac{V_3^k}{h_k} \tag{12}$$

where V_3^k is the applied voltage across the kth layer and h_k is the thickness of the kth layer.

Using Eq. (6) in Eq. (5), the sensor equation can be written as

$$\{D\}_k = [d][Q]_k\{\varepsilon\}_k + [\hat{\varepsilon}]_k\{E\}_k \tag{13}$$

Since the z-axis is the poling axis, the charge is collected only in the z-direction, and hence only D_3^k is considered. The applied electric voltage V_3^k is zero (and hence $E_3^k = 0$) for a piezoceramic sensor layer. Using Eq. (2) in Eq. (13), the expression for D_3^k can be written as (Lee, 1990)

$$D_3^k = \{\overline{d}\}_k^{\mathrm{T}}[\overline{Q}]_k\{\overline{\varepsilon}\}_k \tag{14}$$

The charge measured through the electrodes of a sensor patch in the kth layer is given by

$$q = \frac{1}{2}\left[\left(\int_R D_3^k \mathrm{d}A\right)_{z=z_k} + \left(\int_R D_3^k \mathrm{d}A\right)_{z=z_{k-1}}\right] \tag{15}$$

where R is the effective surface electrode of the patch. The effective surface electrode is the portion of the patch that is covered by electrodes on both sides. The electric charge generated due to the external mechanical disturbance will be detected only if the charge is collected through the effective surface electrode. In the present study, it is assumed that the entire piezoelectric patch serves as the effective surface electrode.

Substituting Eqs. (2) and (14) in Eq. (15), the equation for charge can be written as

$$q = \int_R \{\overline{d}\}_k^{\mathrm{T}} [\overline{Q}]_k [H]\{u\}\,\mathrm{d}A \tag{16}$$

where $[H]$ is the derivative operator matrix given by

$$[H] = \begin{bmatrix} d_x & 0 & \bar{z}_k^3 d_x & (z_k^0 + \bar{z}_k^3)d_x \\ 0 & 0 & 1 + \bar{z}_k^2 & \bar{z}_k^2 \end{bmatrix} \tag{17}$$

and

$$\begin{aligned} d_x &= \frac{\mathrm{d}}{\mathrm{d}x}; \quad z_k^0 = (z_k + z_{k-1})/2 \\ \bar{z}_k^3 &= -\frac{4}{3h^2}\left(z_k^3 + z_{k-1}^3\right)/2 \\ \{u\} &= \left\{u, w, \frac{\partial w}{\partial x}, \phi_x\right\}^{\mathrm{T}}; \quad \bar{z}_k^2 = \frac{-4}{h^2}\left(z_k^2 + z_{k-1}^2\right)/2 \end{aligned} \tag{18}$$

3. Finite-element formulation

Hamilton's principle is used to derive the equations of motion for the laminated composite beam with integrated piezoelectric sensors and actuators shown in Fig. 1. Hamilton's principle states that

$$\int_{t_1}^{t_2} (\delta T - \delta U + \delta W)\,\mathrm{d}t = 0 \tag{19}$$

where t_1 and t_2 are two arbitrary time instants, T is the kinetic energy, U is the strain energy, W is the work done by external forces and δ denotes the first variation.

The variation in the kinetic energy of the beam can be written as

$$\delta T = \int_L \{\delta \dot{u}\}^{\mathrm{T}} [\overline{M}]\{\dot{u}\} b\,\mathrm{d}x \tag{20}$$

where

$$[\overline{M}] = \begin{bmatrix} I_1 & 0 & 0 & 0 \\ 0 & I_1 & 0 & 0 \\ 0 & 0 & \overline{I}_7 & \overline{I}_1 \\ 0 & 0 & \overline{I}_1 & \overline{I}_2 \end{bmatrix} \tag{21}$$

$$\begin{aligned}\bar{I}_1 &= \frac{16}{9h^4} I_7 - \frac{4}{3h^2} I_5 \\ \bar{I}_2 &= I_3 + \frac{16}{9h^4} I_7 - \frac{8}{3h^2} I_5 \\ \bar{I}_7 &= \frac{16}{9h^4} I_7\end{aligned} \tag{22}$$

and

$$(I_1, I_3, I_5, I_7) = \rho \int_{-h/2}^{h/2} (1, z^2, z^4, z^6)\, \mathrm{d}z$$

The variation in strain energy is given by

$$\delta U = \int_L \left(\{\delta\varepsilon\}^{\mathrm{T}} \{N\} + \delta\gamma_{xz}^0 Q_{xz} + \delta\kappa_{xz} R_{xz} \right) b\, \mathrm{d}x \tag{23}$$

where

$$\{N\} = \{N_x M_x P_x\}^{\mathrm{T}} \tag{24a}$$

and

$$\{\varepsilon\} = \{\varepsilon_x^0 \kappa_x^1 \kappa_x^2\}^{\mathrm{T}} \tag{24b}$$

The virtual work done by external forces is given by

$$\delta W = \int_L f\, \delta w\, b\, \mathrm{d}x \tag{25}$$

where $f = f(x,t)$ is the uniformly distributed load.

The generalized displacements are interpolated by using expressions of the form

$$\begin{aligned}u(x,t) &= \sum_{j=1}^{2} u_j(t) N_j(x) \\ w(x,t) &= \sum_{j=1}^{4} w_j(t) \psi_j(x) \\ \phi(x,t) &= \sum_{j=1}^{2} \phi_j(t) N_j(x)\end{aligned} \tag{26}$$

where N_j are the linear Lagrange interpolation functions and ψ_j are the Hermite cubic interpolation functions. The element equations are obtained by substituting Eq. (26) in Eq. (19). The element equation can be written as

$$[M]^{\mathrm{e}} \{\ddot{\Delta}\}^{\mathrm{e}} + [K]^{\mathrm{e}} \{\Delta\}^{\mathrm{e}} = \{F\}_{\mathrm{ex}}^{\mathrm{e}} + [P_{\mathrm{ac}}]^{\mathrm{e}} V_{\mathrm{p}}^{\mathrm{e}} \tag{27}$$

where $[M]^{\mathrm{e}}$ is the element mass matrix, $[K]^{\mathrm{e}}$ is the element stiffness matrix, $\{F\}_{\mathrm{ex}}^{\mathrm{e}}$ is the element applied-load vector, $[P_{\mathrm{ac}}]^{\mathrm{e}}$ is the element piezoelectric force vector which maps the applied actuator voltage to induced displacements, $V_{\mathrm{p}}^{\mathrm{e}}$ is the voltage applied to the piezoelectric actuator and $\{\Delta\}^{\mathrm{e}}$ is the vector of nodal displacements.

Using the generalized displacements given by Eq. (26) in Eq. (16), the sensor output equation for the ith sensor element can be written as

$$q_i = [S]^e \{\Delta\}^e \tag{28}$$

where $[S]^e$ is the transformation matrix that transforms the nodal displacements to the measured sensor charge.

Assembling Eq. (27) and treating each distributed actuator as an independent actuator, the equations of motion can be written as

$$[M]\{\ddot{\Delta}\} + [K]\{\Delta\} = \{F\}_{ex} + [P_{ac}]\{V\}_{ac} \tag{29}$$

where $\{\Delta\}$ is a $(4n \times 1)$ vector of nodal displacements, $\{\ddot{\Delta}\}$ is a $(4n \times 1)$ vector of nodal accelerations, $[M]$ is a $(4n \times 4n)$ global mass matrix, $[K]$ is a $(4n \times 4n)$ global stiffness matrix, $\{F\}_{ex}$ is a $(4n \times 1)$ global force vector, $[P_{ac}]$ is a $(4n \times P)$ transformation matrix that transforms the actuator voltage to the actuator force, $\{V\}_{ac}$ is a $(P \times 1)$ vector of actuator voltages, n is the number of nodes in the mesh and P is the number of independent actuators.

In order to include the effects of structural damping, the above equations are modified as follows:

$$[M]\{\ddot{\Delta}\} + [C]\{\dot{\Delta}\} + [K]\{\Delta\} = \{F\}_{ex} + [P_{ac}]\{V\}_{ac} \tag{30}$$

where $[C]$ is the damping matrix and can be expressed as

$$[C] = \alpha[K] + \beta[M] \tag{31}$$

The constants α and β are the damping parameters (Bathe, 1996).

Treating the distributed sensors as independent sensors, the sensor output equations can be written as

$$\{q\} = [S]\{\Delta\} \tag{32}$$

where $\{q\}$ is a $(\gamma \times 1)$ vector of sensor outputs, $[S]$ is a $(\gamma \times 4n)$ transformation matrix that transforms the nodal displacement to the measured sensor charge, $\{\Delta\}$ is a $(4n \times 1)$ vector of nodal displacements, n is the number of nodes in the mesh and γ is the number of independent piezoelectric sensors.

4. Adaptive neuro-controller design

The adaptive control neuro-architecture consists of two neural networks as shown in Fig. 2, namely the identifier network (Fig. 4) and the controller network (Fig. 5). Each network is made up of an input layer, a hidden layer and an output layer. The identifier network is a feed forward neural network while the neuro-controller is a diagonal recurrent neural network. The inputs to the identifier are the actuator voltages $\{V_{ac}(t)\}$ (output of the neuro-controller) and the sensor voltages $\{V_s(t-1)\}$. The identifier then outputs the new predicted sensor voltages $\{\overline{V}_s(t)\}$. The inputs to the neuro-controller are sensor voltages $\{V_s(t-1)\}$ and actuator voltages $\{V_{ac}(t-1)\}$. In general, a set of 'M' previous available actuator and sensor voltages are used for identifier network and neuro-controller. The outputs of the neuro-controller are the new actuator voltages $\{V_{ac}(t)\}$. The number of neurons in the input and output layers of the two neural networks is determined by the number of sensors and actuators used in controlling the beam.

4.1. Identifier

In practice, the identifier can be connected in parallel with the structure until the desired training is achieved. The identifier is trained such that $V_s(t) \approx \overline{V}_s(t)$, i.e., the identifiers predicted sensor voltages match with the actual beam dynamics. The finite element model is used to generate the requisite data by driving the actuators with sinusoidal signals having an amplitude of 200 V and frequencies equal to the first two natural frequencies. Since the output of the plant rather than the identifier is fed back, static back prop-

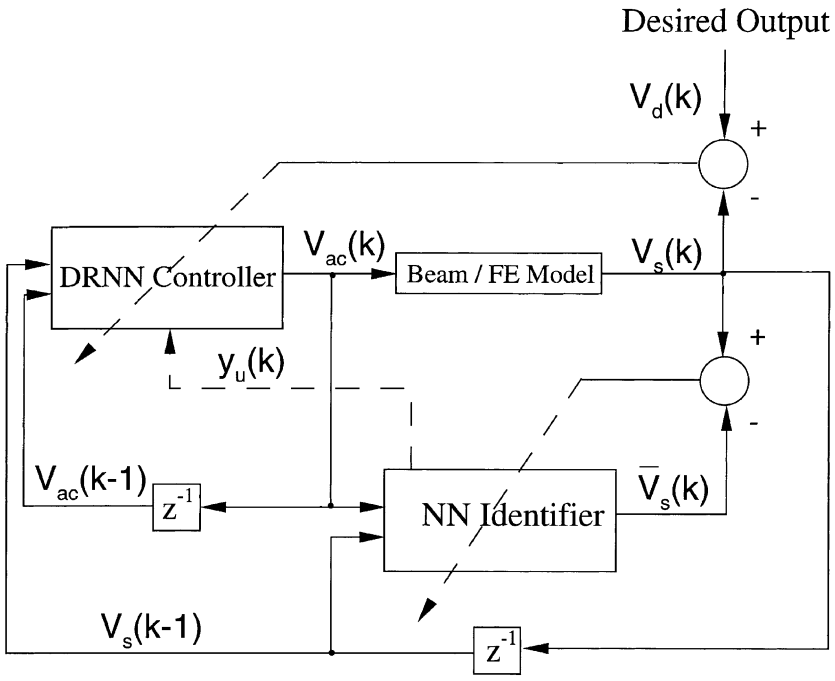

Fig. 2. Block diagram of the hybrid control system.

agation can be used to update the identifier weights. The following is a brief overview of static back propagation theory.

Back propagation networks are feed forward networks consisting of an input layer, one or more hidden layers and an output layer (Haykin, 1994). Each neuron in a layer is connected to all neurons in the immediately preceding and following layers. The weights associated with the connections are updated such that the neural network gives the desired output for the given input. The neural network weights are initialized to small random values in the range ± 1 to start the training. The training set consists of input vectors and corresponding desired output vectors. The values of the inputs and outputs are normalized between ± 1. The activity of a neuron is determined as shown in Fig. 3. The total weighted input to a typical neuron k is

$$\mathrm{net}_k = \sum_{i=1}^{N} w_{ki} z_i \tag{33}$$

where z_i is the output of the ith neuron in the previous layer, w_{ki} is the weight of the connection between the ith and kth unit and N is the total number of neurons in the previous layer. The output of the neuron is a function of the total weighted input. The input and output layers of the identifier use a linear threshold function, meaning that the output of the neuron is the same as its total weighted input value. Hidden layer neurons use a bipolar sigmoidal function defined as

$$z_j = \frac{2}{1 + e^{-\mathrm{net}_j}} - 1 \tag{34}$$

where z_j is the output of the jth hidden layer neuron and net_j is the total weighted input to the neuron.

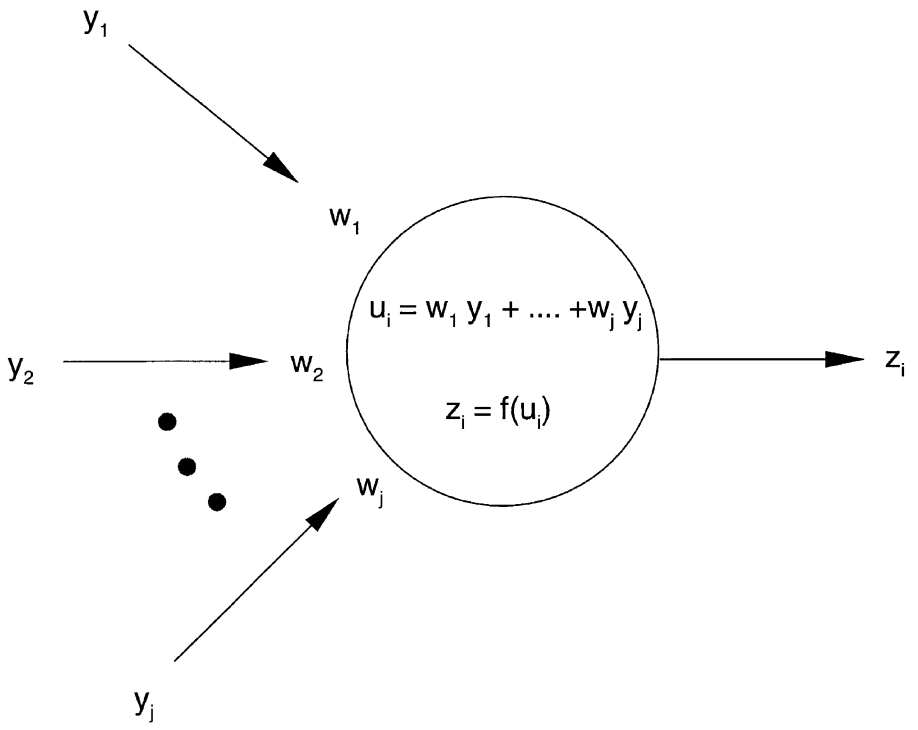

Fig. 3. Activity of a neuron.

Once the output activity $\overline{V}_{sk}$ for all output layer neurons has been determined it can be compared to the expected output V_{sk} for training purposes. The total error of the network is defined as

$$E = \frac{1}{2}\sum_{k=1}^{N_o}(\overline{V}_{sk} - V_{sk})^2 = \frac{1}{2}\sum_{k=1}^{N_o}\delta_{ok}^2 \tag{35}$$

where N_o is the number of neurons in the output layer which is equal to the number of sensors and, $\delta_{ok} = (\overline{V}_{sk} - V_{sk})$. The training continues until the error is within acceptable limits. The weights of the kth output layer for a network with N_o output nodes and N_h hidden layer nodes is adjusted as follows:

$$w_{kj}^o(t+1) = w_{kj}^o(t) + \eta\delta_{ok}z_j \tag{36}$$

where $k = 1,\ldots,N_o$, $j = 1,\ldots,N_h$, η is the learning rate which is generally between 0.01 and 1, and z_j is the output of the jth neuron of the hidden layer. Similarly, the weights for the jth hidden layer for a network with N_h hidden layer nodes and N_i input nodes is updated using

$$v_{ji}(t+1) = v_{ji}(t) + \eta f_j'(\mathrm{net}_j)z_i\sum_{k=1}^{N_o}\delta_{ok}w_{kj} \tag{37}$$

where $j = 1,\ldots,N_h$ and $i = 1,\ldots,N_i$. The schematic of the NN identifier is given in Fig. 4.

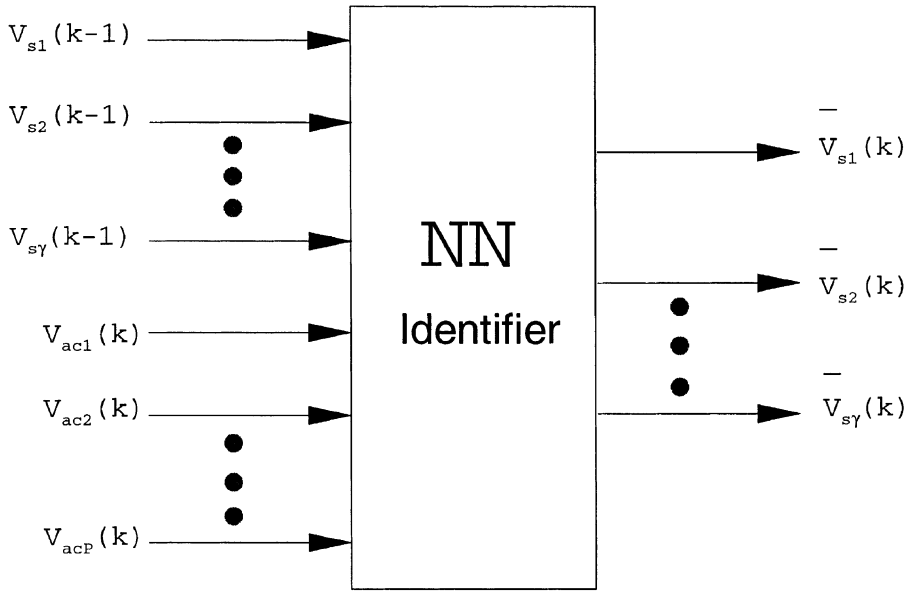

Fig. 4. Schematic of neural network identifier.

4.2. Diagonal recurrent neural network controller

The DRNN is shown in Fig. 5. Let M_i, M_h, M_o be the number of neurons in the input, hidden and output layers, respectively. Then the mathematical model for the DRNN is defined as (Ku and Lu, 1995; Narendra and Parthasarathy, 1990)

$$\begin{aligned} V_{ac_k}(t) &= O_k(t) = \sum_{j}^{M_h} W_{kj} Y_j(t); \quad Y_j(t) = f(\mathrm{net}_j(t)) \\ \mathrm{net}_j(t) &= W_j^R Y_j(t-1) + \sum_{i=1}^{M_i} V_{ji} I_i(t) \end{aligned} \tag{38}$$

where for each time instant t, $I_i(t)$ is the ith input to the DRNN, $\mathrm{net}_j(t)$ is the sum of inputs to the jth recurrent neuron, $Y_j(t)$ is the output of the jth recurrent neuron, and $O_k(t) = V_{ac_k}(t)$ is the output of the kth output neuron which is the same as the kth actuator input. Here $f(\cdot)$ is the bipolar sigmoid function, and V_{ji}, W_j^R, and W_{kj} are input, recurrent, and output weights, respectively.

The error function for the DRNN controller is defined as

$$E_c = \frac{1}{2} \sum_{m=1}^{M_o} (V_{dm}(t) - V_{sm}(t))^2 \tag{39}$$

where $V_{dm}(t)$ and $V_{sm}(t)$ are the desired and actual responses of the structure and γ is the number of sensor outputs from the structure. The controller weights are updated according to

$$W^c(t+1) = W^c(t) + \eta \left(\frac{-\partial E_c}{\partial W^c} \right) \tag{40}$$

where W^c represent W_{kj}, W_j^R or V_{ji}

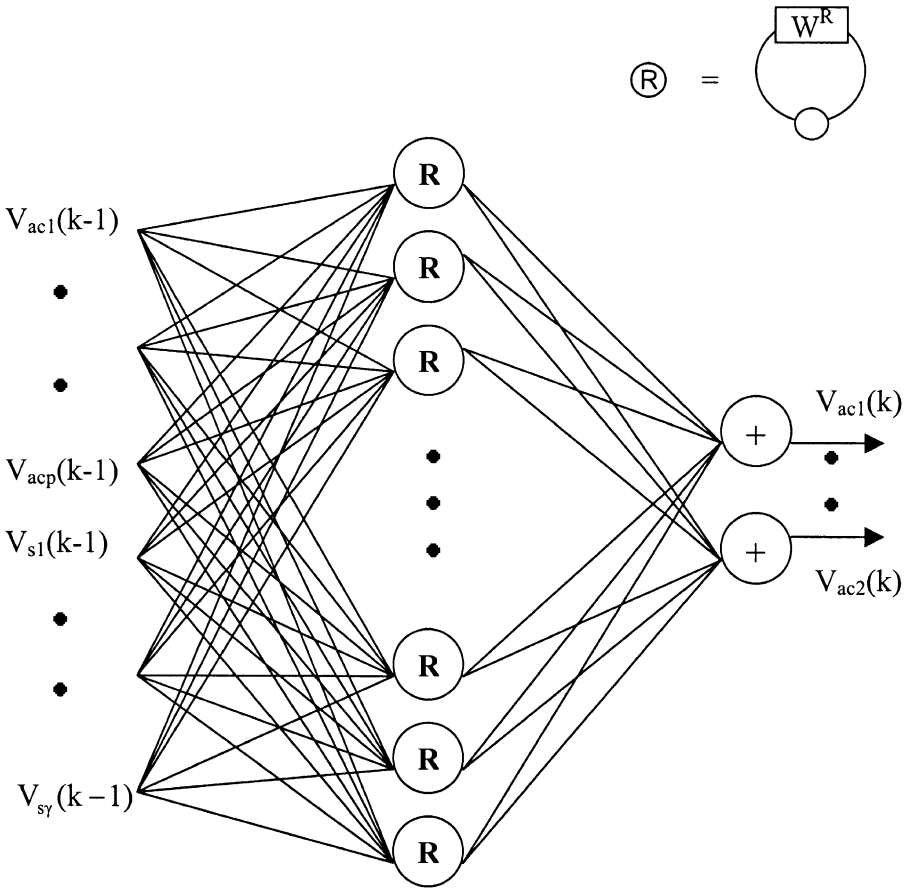

Fig. 5. DRNN controller.

$$\frac{\partial E_{\mathrm{c}}}{\partial W^{\mathrm{c}}} = -\sum_{m=1}^{M_{\mathrm{o}}} e_{\mathrm{c}m}(t)\frac{\partial y_m(t)}{\partial W^{\mathrm{c}}} = -\sum_{m=1}^{M_{\mathrm{o}}} e_{\mathrm{c}m}(t)\left(\sum_{k=1}^{N_{\mathrm{o}}}\frac{\partial V_{sm}(t)}{\partial V_{\mathrm{ac}_k}(t)}\frac{\partial V_{\mathrm{ac}_k}(t)}{\partial W^{\mathrm{c}}}\right) \tag{41}$$

where $e_{\mathrm{c}m} = (V_{\mathrm{d}m}(t) - V_{sm}(t))$ and $\partial V_{sm}(t)/\partial V_{\mathrm{ac}_k}(t)$ is the sensitivity of the mth output of the structure (mth sensor voltage) with respect to the kth input (actuator voltage). Since the system dynamics are usually unknown, the sensitivity is unknown. However, this can be estimated using the neural identifier. After the identifier is sufficiently trained, the dynamic behavior of the identifier is close to that of the structure, i.e., $V_{sm} \approx \overline{V}_{sm}$, where $\overline{V}_{sm}$ is the output of the identifier. Hence we assume the sensitivity can be approximated as

$$\frac{\partial V_{sm}(t)}{\partial V_{\mathrm{ac}_k}(t)} \approx \frac{\partial \overline{V}_{sm}(t)}{\partial V_{\mathrm{ac}_k}(t)} \tag{42}$$

Applying the chain rule to Eq. (41) and using Eq. (42), gives for the configuration used

$$\frac{\partial E_{\mathrm{c}}}{\partial W_{kj}} = -\sum_{m=1}^{M_{\mathrm{o}}} e_{\mathrm{c}m}\left(\sum_{l=1}^{N_{\mathrm{i}}} v_{ml} f'(\mathrm{net}_l(t)) w_{kl}\right) Y_j \tag{43}$$

$$\frac{\partial E_c}{\partial W_j^R} = -\sum_{m=1}^{M_o} e_{cm}\left(\sum_{k=1}^{N_o}\left(\sum_{l=1}^{N_i} v_{ml} f'(\mathrm{net}_l(t)) w_{kl}\right) W_{kj} P_j(t)\right) \tag{44}$$

$$\frac{\partial E_c}{\partial V_{ji}} = -\sum_{m=1}^{M_o} e_{cm}\left(\sum_{k=1}^{N_o}\left(\sum_{l=1}^{N_i} v_{ml} f'(\mathrm{net}_l(t)) w_{kl}\right) W_{kj} Q_{ij}(t)\right) \tag{45}$$

where

$$P_j(t) = f'(\mathrm{net}_j(t))[Y_j(t-1) + W_j^R P_j(t-1)]; \quad P_j(0) = 0 \tag{46}$$

$$Q_{ij}(t) = f'(\mathrm{net}_j(t))[I_i(t) + W_j^R Q_{ij}(t-1)]; \quad Q_{ij}(0) = 0 \tag{47}$$

5. Results and discussion

The NN identifier was trained offline using 3000 input–output pairs generated using the finite element model. Sinusoidal actuator voltages of amplitude 200 V and frequencies equal to the first two modal frequencies were used for the generation of training data. The identifier was trained until the normalized mean-square error was below 0.01. Once the identifier was trained to within acceptable limits the hybrid

Table 1
Material and geometric data

	T300/5208 graphite/epoxy	PKI 502 (sensor)	PKI 404 (actuator)
E_1 (GPa)	174.8	71.0	80.0
E_2 (GPa)	10.3	71.0	80.0
G_{12} (GPa)	7.17	28.4	32.0
G_{13} (GPa)	7.17	28.4	32.0
G_{23} (GPa)	6.21	28.4	32.0
v_{12}	0.25	0.25	0.25
ρ (kg/m^3)	1389.23	7600.0	7500.0
d_{31} (m/V)	–	-175×10^{-12}	-150×10^{-12}
d_{32} (m/V)	–	-175×10^{-12}	-150×10^{-12}
Length (m)	1.0	0.1	0.1
Width (m)	0.0254	0.0254	0.0254
Thickness (m)	0.0127	0.0002	0.0002

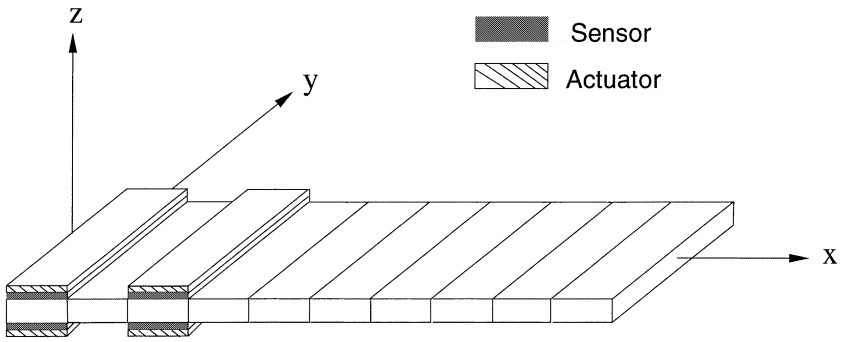

Fig. 6. Layout of the beam showing element discretization and collocated sensor and actuator locations.

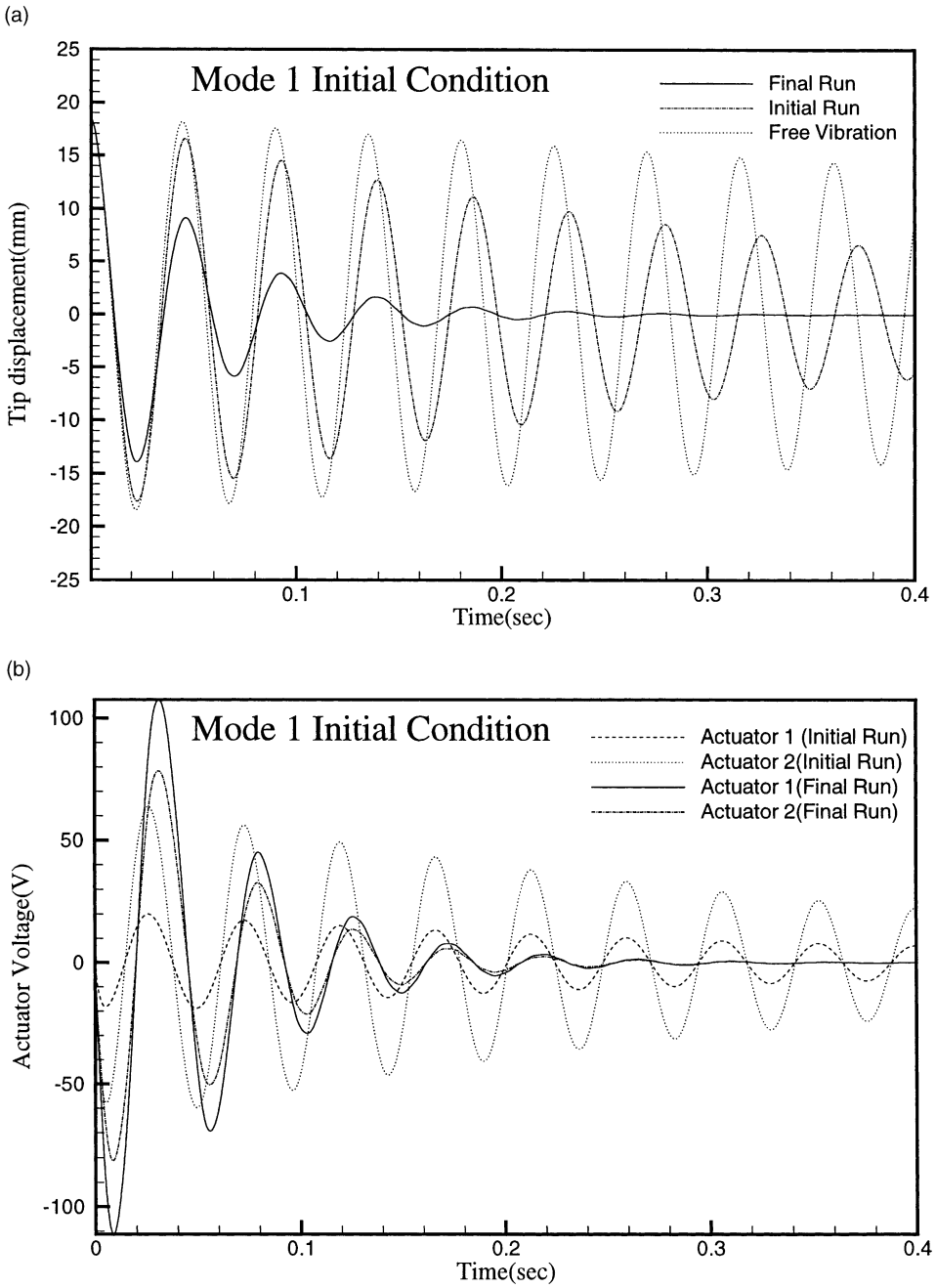

Fig. 7. Hybrid controller performance as learning progresses.

system was assembled. The training of the identifier is however continued during the subsequent test runs. The DRNN controller is initialized to random weights between 0 ± 0.01. Approximately 10 arbitrary sinusoidal excitations were given to the structure to learn the DRNN controller weights. Subsequently, the test simulations were carried out.

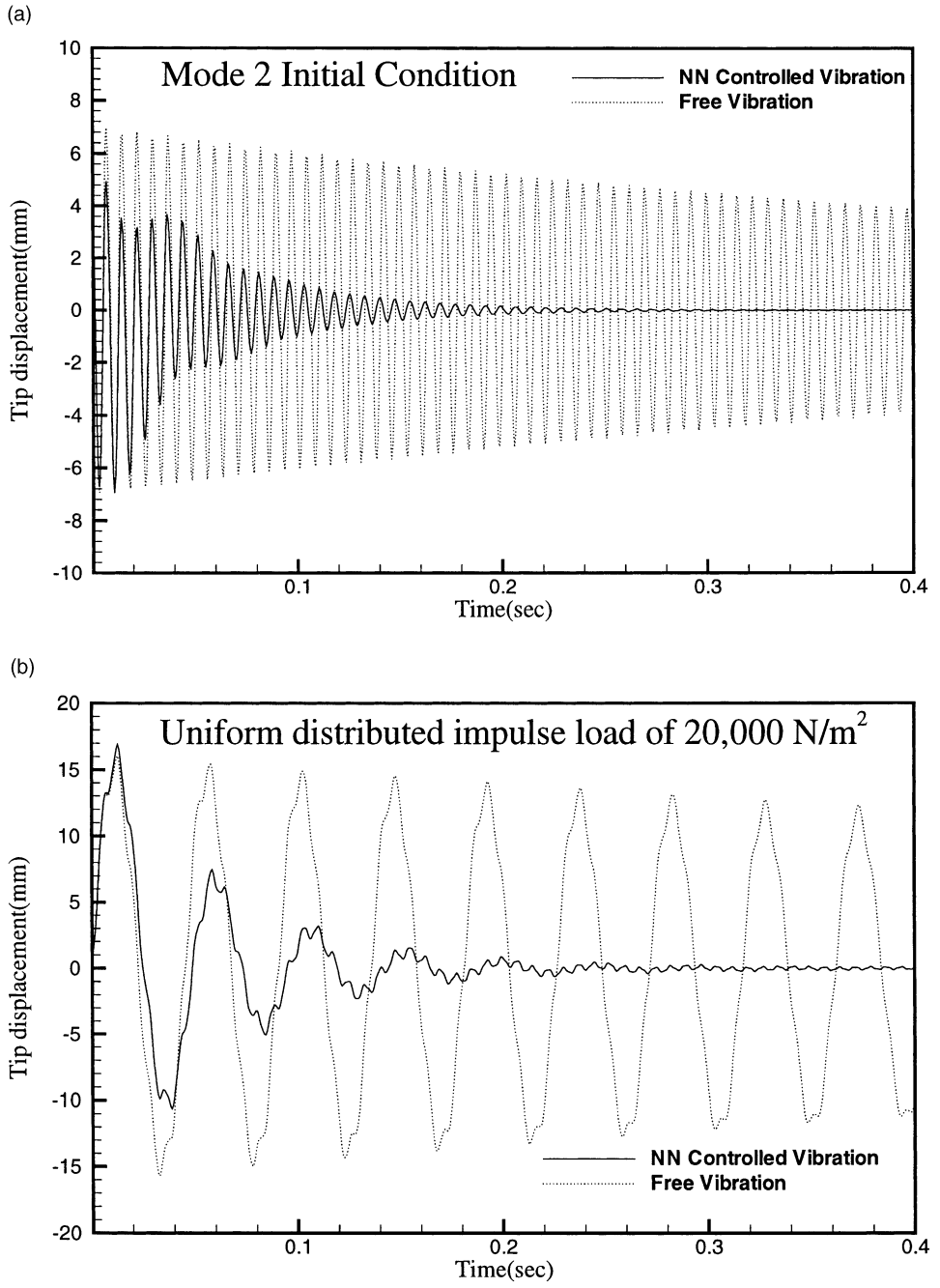

Fig. 8. Controller performance for different excitations.

The performance of the hybrid control system was tested for various initial conditions and loadings. The properties of the smart composite beam are given in Table 1. The beam is discretized into 10 finite elements. Two independent collocated sensors and actuators are located as shown in Fig. 6. As a result the controller

and the identifier have two output neurons each. The identifier network is trained with 20 hidden layers while the controller network is trained with 10 hidden layers. The sensors are bonded to the top and bottom surfaces of the beam, and the actuators are bonded on top of the sensors. The two collocated actuator layers are polarized in opposite directions in order to generate only bending moments. For all cases a four-layer [0°/90°/90°/0°] beam with clamped-free boundary conditions is considered. The origin in Fig. 6 corresponds to the clamped end. The controller and identifier networks are updated during each test run. Hence each test run utilizes the updated networks obtained from the previous run unless otherwise mentioned.

Fig. 7(a) shows the controller performance for a mode 1 initial condition. It can be seen that the performance improves as the training of the controller progresses. Fig. 7(b) shows the corresponding actuator voltages at each stage of the training. Fig. 8(a) and (b) show the controller performance for a mode 2 initial condition and a uniform distributed impulsive load of 20,000 N/m^2 acting for 0.001 s, respectively. Here again the controller is successful in damping out the vibrations.

The robustness of the proposed system is examined for various system parameter variations. The beam is excited by an initial condition corresponding to the first mode of vibration of the original system for all of the cases considered in the parameter variation study. The results are shown in Fig. 9. Fig. 9(a) shows the free vibration response for the cases considered. For the increased frequency case $E_1 = 204.9$ GPa and $\rho = 1189.23$ kg/m^3 while the other parameters are unchanged from the original system. For the decreased

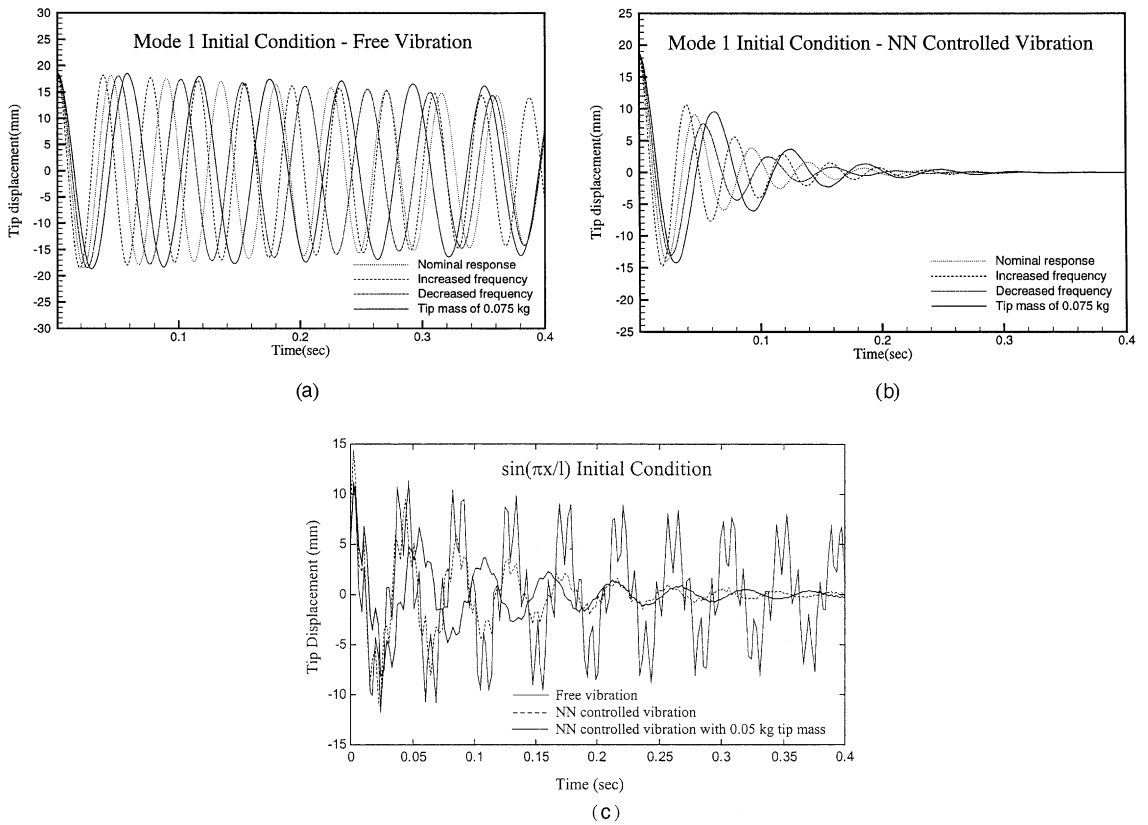

Fig. 9. Robustness study – effect of structural parameter variation.

frequency case $E_1 = 154.9$ GPa and $\rho = 1589.23$ kg/m^3. In the third case a tip mass of 0.075 kg is used. In all cases it can be seen that the NN-controller is successful in damping out the vibration. Moreover, the settling time for all the cases is close to the nominal case which shows the robustness of the controller. Fig. 9(c) shows the case of free-vibration damping with sinusoidal initial condition and a tip mass of 0.5 kg. Sinusoidal initial condition is taken proportional to $\sin(\pi x/l)$ so that it excites almost all modes of vibrations. First and second modes of vibration are clearly visible in free span-loop vibration. Both the modes are successfully damped by the recurrent neuro-controller.

Next, the robustness was studied for loss of sensing or actuation. Fig. 10(a) shows the free and NN-controlled responses for a mode 1 initial condition with sensor 2 offline. Sensor 2 corresponds to the one on the third element from the clamped end. Fig. 10(b) shows the response with actuator 2 disabled. Actuator 2 again corresponds to the third element from the clamped end. The degradation in performance with partial sensor feedback is negligible. As expected the deterioration in performance is more marked when the actuator 1 is taken offline. However, even in this case the performance of the neuro-control system is satisfactory. Fig. 10(c) shows the case where actuator 1 and sensor 2 are off line. Thus the beam simulates a non-collocated actuator and sensor scenario. Even in this case the performance of the controller is satisfactory.

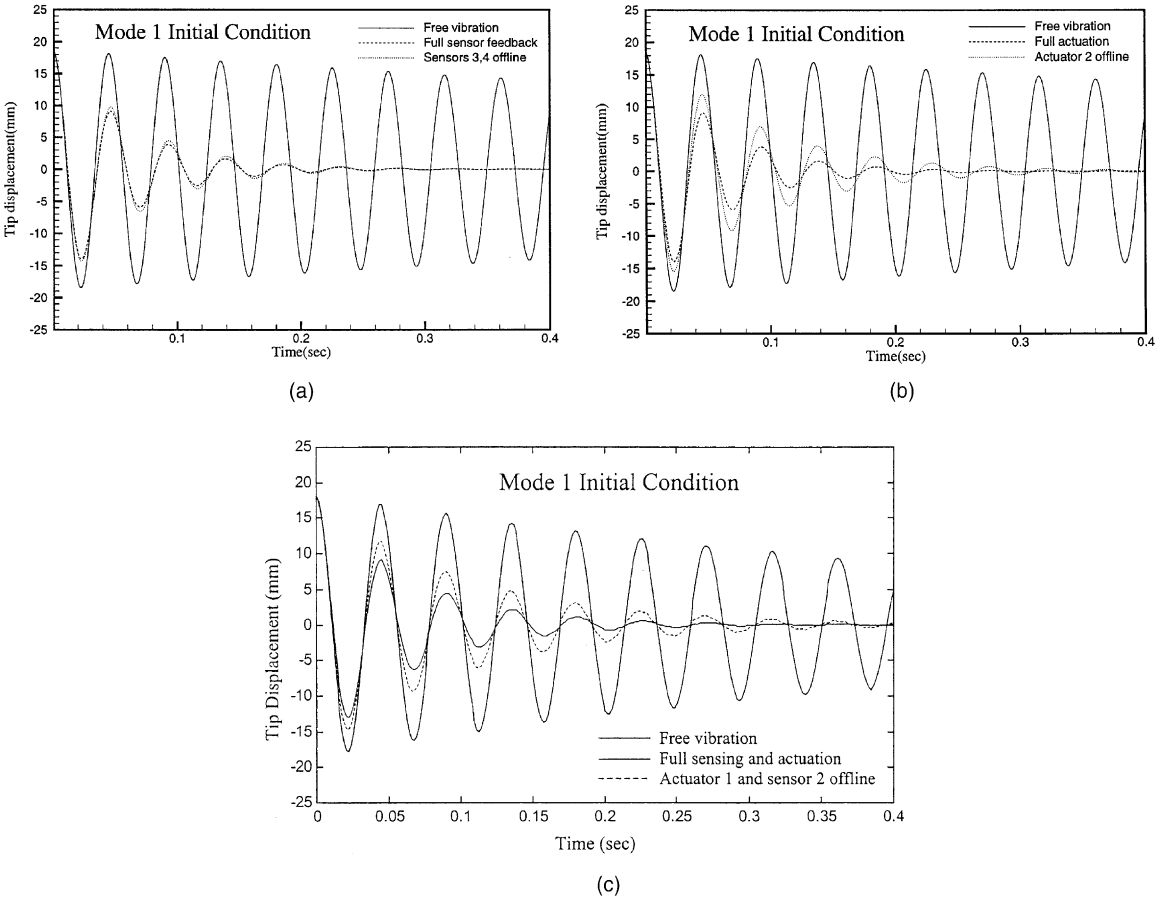

Fig. 10. Robustness study – effect of partial loss of sensor output or actuation.

6. Conclusions

Vibration control of smart composite beams using a self-adaptive neural-controller was studied. A finite element model based on a higher-order shear deformation theory was developed to simulate the vibration of the composite beam. The neural network identifier was trained offline using data generated by the finite element model. The DRNN controller was trained online while the identifier itself learns quasi-static changes in system dynamics. Simulations were carried out to study the performance and robustness of the neural-control system for different initial conditions, structural parameter variations and loss of sensing or actuation. The recurrent control architecture was shown to perform effectively and robustly in all the cases studied.

References

Bathe, K.J., 1996. Finite Element Procedures. Englewood Cliffs, Prentice-Hall, NJ.

Bhimaraddi, A., Chandrashekhara, K., 1991. Some observations on the modelling of laminated composite beams with general lay-ups. Composite Structures 9, 371–380.

Boussalis, D., Wang, S.J., 1993. Multivariable neural network vibration control based on output feedback. Proceedings of Second IEEE Conference on Control Applications 1, 345–350.

Chandrashekhara, K., Agarwal, A.N., 1993. Active vibration control of laminated composite plates using piezoelectric devices: a finite-element approach. Journal of Intelligent Materials Systems and Structures 4, 496–508.

Chen, C.I., 1994. Active vibration control using the modified independent modal space control (MIMSC) algorithm and neural networks as state estimators. Journal of Intelligent Materials Systems and Structures 5, 550–558.

Crawley, E.F., de Luis, J., 1987. Use of piezoelectric actuators as elements of intelligent structures. AIAA Journal 29, 1373–1385.

Damle, R., Rao, V., 1997. Real-time adaptive control of nonlinear smart structure systems using neural networks. Proceedings of SPIE Conference on Smart Structures and Materials: Mathematics and Control in Smart Structures 3039, 34–39.

Flanders, S.W., Burke, L.I., Yalcintas, M., 1994. Alternate neural network architectures for beam vibration minimization. Adaptive Structures and Composite Materials: Analysis and Applications AD-45/MD-54, 293–298.

Haykin, S., 1994. Neural Networks: A Comprehensive Foundation. Macmillan, New York, NY.

Ku, C., Lee, K.Y., 1995. A diagonal recurrent neural networks for dynamic systems control. IEEE Transactions on Neural Networks 6, 144–155.

Lee, C.K., 1990. Theory of laminated piezoelectric plates for the design of distributed sensors/actuators. Part I: Governing equations and reciprocal relationships. Journal of Acoustical Society of America 87, 1144–1158.

Narendra, K.S., Parthasarathy, K., 1990. Identification and control of dynamical systems using neural networks. IEEE Transactions on Neural Networks 1, 4–27.

Smyser, C.P., Chandrashekhara, K., 1997. Robust vibration control of composite beams using piezoelectric devices and neural networks. Smart Material and Structures 4, 178–189.

Varadarajan, S., Chandrashekhara, K., Agarwal, S., 2000. LQG/LTR based robust control of composite beams with piezoelectric devices. Journal of Vibration and Control 6, 607–630.